

Title	Experimental and numerical study on transient elongational viscosity for PP/LDPE blends
Author(s)	Otsuki, Yasuhiko; Fujii, Yoko; Sasaki, Hiroko; Phulkerd, Panitha; Yamaguchi, Masayuki
Citation	Polymer Journal, 52(5): 529-538
Issue Date	2019-11-21
Type	Journal Article
Text version	author
URL	http://hdl.handle.net/10119/16965
Rights	This is the author-created version of Springer, Yasuhiko Otsuki, Yoko Fujii, Hiroko Sasaki, Panitha Phulkerd, Masayuki Yamaguchi, Polymer Journal, 52(5), 2019, 529-538. The original publication is available at www.springerlink.com , https://doi.org/10.1038/s41428-019-0286-0
Description	

Experimental and Numerical Study on Transient Elongational Viscosity for PP/LDPE Blends

Yasuhiko Otsuki,^{1*} Yoko Fujii,² Hiroko Sasaki,¹ Panitha Phulkerd,²
and Masayuki Yamaguchi^{2*}

1) Packing and Industrial Materials Laboratory,
Prime Polymer Co., Ltd.,
3 Chigusa-Kaigan, Ichihara, Chiba 299-0108 JAPAN

2) School of Materials Science,
Japan Advanced Institute of Science and Technology
1-1 Asahidai, Nomi, Ishikawa 923-1292 JAPAN

Running Head: Elongational Viscosity of PP/LDPE

* Corresponding to

Yasuhiko Otsuki (Yasuhiko.Otsuki@primepolymer.co.jp)

1 Masayuki Yamaguchi (m_yama@jaist.ac.jp)

2 **Abstract**

3 The transient uniaxial elongational viscosity for binary blends composed of
4 polypropylene (PP) and low-density polyethylene (LDPE) was evaluated. A strain
5 hardening behavior is detected for the blends, although LDPE is a dispersed phase. This
6 behavior is attributed to LDPE dispersion deformation; the LDPE forms rigid fibers
7 because of strain hardening. Rheological properties are calculated numerically by the
8 Phan–Thien Tanner model by assuming a symmetric geometry with a periodic structure.
9 Based on the simulation, we propose an appropriate LDPE to modify the processability
10 of PP, at which the strain hardening in the elongational viscosity is required.

11

12 **Keywords:** polypropylene / low-density polyethylene / elongational viscosity /
13 numerical simulation / viscoelasticity

14

15 **1. Introduction**

16 Polymer blending is one of the most important technologies that supports the
17 modern plastics industry and can improve product performance, such as mechanical and
18 thermal properties. Rheological property modification is another target of polymer
19 blending to enhance the processability at various processing operations. The ability to
20 increase the melt elasticity of a linear polymer is in strong demand in the industry.
21 Several methods have been proposed to provide strain hardening in elongational
22 viscosity, which is an important elastic property [1-10]. Among them, the simple
23 addition of commercially available low-density polyethylene (LDPE) to isotactic
24 polypropylene (PP) should be noted for potential industrial application [10]. In a
25 previous study in which PP/LDPE blends were used, LDPE showed a slightly lower
26 shear viscosity than PP, and it was suggested that the deformed LDPE droplets that were
27 dispersed in the molten PP become rigid because of LDPE strain hardening during
28 uniaxial elongational flow. Consequently, the blend behaved like a composite with rigid
29 fibers, and led to a rapid increase in the elongational viscosity owing to the excess stress
30 generation of a matrix between the fibrous dispersions [11-13]. Therefore, the viscosity
31 ratio of the components, i.e., PP and LDPE, should have an important effect on the
32 elongational viscosity of the blend systems, although such an effect has not been

33 revealed yet. One of the main purposes of this work is to clarify the effect of viscosity
34 ratio on the strain hardening behavior in the transient elongational viscosity for
35 PP/LDPE blends. We also study the growth curves of elongational viscosity for
36 PP/LDPE blends by numerical simulation based on the mechanism mentioned above.
37 Because measurement data of elongational viscosity often contain experimental error,
38 predicted results by the numerical simulation should be considered seriously. In terms of
39 PP processability, we proposed an appropriate LDPE as a processing modifier based on
40 the simulation.

41 To date, considerable theoretical work has been conducted on two-phase flow
42 that consists of a matrix and dispersions in polymer blends. Most studies have focused
43 on droplet deformation owing to hydrodynamic force, and droplet breakup and/or
44 coalescence with a consideration of the viscosity ratio, interfacial tension, capillary
45 number, and flow pattern [14-21]. The simulation results provided information on
46 material design and appropriate processing conditions to prepare polymer blends with
47 fine dispersed droplets. In recent years, these research activities have progressed
48 understanding, such as the simulation of mechanical behaviors of individually dispersed
49 droplets in a three-dimensional space [22] and an analysis of complicated
50 three-dimensional droplet deformation [23]. However, numerical studies on the

51 relationship between the structure of multiphase fluids and melt viscoelasticity has not
52 been carried out extensively. In terms of elongational viscosity, several studies were
53 reported for a suspension system with rigid particles dispersed in a viscous fluid [24-26].
54 In these studies, flow simulations were performed for a suspension with a number of
55 randomly dispersed rigid particles, and the simulations agreed well with the
56 experimental data for planar elongational flow. If we consider the calculation cost and
57 practical use, however, the calculation of a microstructural unit with one or two particles
58 based on an assumption of the periodic existence of particles is preferred to predict the
59 viscoelastic properties of a whole system. When rigid particles are arranged periodically
60 under uniaxial elongational flow, however, they approach each other in the transversal
61 direction to the flow, which leads to an unrealistic calculated result. Therefore, it is
62 necessary to set rigid particles that are arranged randomly in the matrix. When particles
63 are not rigid, they show a large deformation; in contrast, such an unrealistic structure
64 will not occur even under a large deformation. Consequently, an approximation of the
65 initial periodic structure will be kept until the final stage of deformation, which suggests
66 that viscoelastic properties of a system that contains flexible particles can be predicted
67 by a periodic local model.

68 Here, we carried out experiments using immiscible PP/LDPE blends with

69 various viscosity ratios, in which LDPE particles were dispersed in the PP matrix. The
70 experimental results obtained were compared with numerical simulations, which were
71 performed by assuming a symmetric geometry with a periodic structure. The
72 Lagrangian finite-element method with moving boundaries was used for isothermal
73 creeping-flow simulation. The viscoelastic characteristics of the samples were described
74 by the Phan–Thien Tanner (PTT) model with multiple relaxation modes. The
75 contribution of interfacial tension was ignored because it is insignificant compared with
76 the remarkable strain hardening of LDPE.

77

78 **2. Experimental Procedure**

79 **2.1 Materials**

80 A propylene homopolymer (PP; Primepolymer, Tokyo, Japan) and three types
81 of low-density polyethylene (LDPE) with different shear viscosities were used. The PP
82 melt-mass flow rate was 3.0 g/10 min at 230 °C for 2.16 kg and those of the LDPE were
83 3.7 for LDPE-L, 1.6 for LDPE-M, and 0.3 g/10 min for LDPE-H at 190 °C for 2.16 kg.
84 LDPE-L and LDPE-M were produced by an autoclave reactor, whereas LDPE-H was
85 produced by a tubular reactor. One of the LDPE samples, LDPE-M, and PP were used
86 in our previous study [10].

87 The PP/LDPE blend samples (PP:LDPE = 70:30, weight ratio) were prepared
88 by an internal batch mixer (Labo-Plastmill 10M100, Toyo Seiki Seisaku-sho, Tokyo,
89 Japan), and by rotating the blades at 30 rpm at 190 °C for 3 min, in the presence of
90 5,000 ppm of thermal stabilizers, such as tris(2,4-di-tert-butylphenyl)phosphate
91 (Irgafos168, Ciba, Bazel, Switzerland) and pentaerythritol
92 tetrakis(3-(3,5-di-tert-butyl-4-hydroxyphenyl)propionate) (Irganox1010, Ciba). The
93 blended samples were compressed into flat sheets at 190 °C for 5 min by using a
94 compression-molding machine, and quenched in the cooling unit.

95

96 **2.2 Measurements**

97 A cone-and-plate rheometer (AR2000ex, TA Instruments, New Castle, DW)
98 was used to evaluate the frequency dependence of the shear storage modulus G' and
99 loss modulus G'' at 190 °C. The cone angle was 4° and its diameter was 25 mm. The
100 growth curves of the transient uniaxial elongational viscosity were measured by the
101 rotational rheometer equipped with a universal testing platform (SER2-G, Xpansion
102 Instruments, Tallmadge, OH) at 190 °C. Rectangular 10-mm-wide, 15-mm-long, and
103 0.8-mm-thick samples were used for the measurements.

104

105 3. Numerical Simulation

106 3.1 Governing equations

107 By considering the flow of a highly viscous fluid, ignoring the effects of inertia
 108 and gravity, and assuming that the fluid is isothermal and incompressible, the equation
 109 of motion and the equation of continuity were given by equations (1) and (2),
 110 respectively.

$$111 \quad -\nabla p + \nabla \cdot \boldsymbol{\tau} = \mathbf{0} \quad (1)$$

$$112 \quad \nabla \cdot \mathbf{v} = 0 \quad (2)$$

113 where p is the isotropic pressure, $\boldsymbol{\tau}$ is the stress tensor, and \mathbf{v} is the velocity vector.

114 As the viscoelastic constitutive equation, the PTT model with a multiple
 115 relaxation mode [27] represented by equations (3), (4), and (5) was used, in which the
 116 stress-coefficient function $Y_i(\boldsymbol{\tau}_i)$ was expressed by the exponential form;

$$117 \quad Y_i(\boldsymbol{\tau}_i) \boldsymbol{\tau}_i + \lambda_i \left[\frac{\xi}{2} \boldsymbol{\tau}_i^{\Delta} + \left(1 - \frac{\xi}{2}\right) \boldsymbol{\tau}_i^{\nabla} \right] = 2\eta_{0i} \mathbf{D} \quad (3)$$

$$118 \quad Y_i(\boldsymbol{\tau}_i) = \exp\left(\frac{\zeta}{G_i} \text{tr}(\boldsymbol{\tau}_i)\right) \quad (4)$$

$$119 \quad \boldsymbol{\tau} = \sum_{i=1}^n \boldsymbol{\tau}_i \quad (5)$$

120 where \mathbf{D} is the deformation velocity tensor. $\boldsymbol{\tau}_i$, λ_i , η_{0i} , and G_i are the stress tensor,
 121 relaxation time, zero shear viscosity, and relaxation modulus of the mode i , respectively.

122 The superscript Δ and ∇ represent the lower- and upper-convected time derivatives,
 123 respectively, and ζ and ξ are the non-linear parameters used in the PTT model.

124

125 **3.2 Numerical procedure**

126 We reported previously flow analysis during the stretching of foam with a
 127 moving boundary based on the Galerkin finite-element method [28]. In this study, the
 128 program was expanded to incorporate the dispersed phase as a viscoelastic fluid for the
 129 flow analysis. A Lagrange mesh was used, in which the positions of the nodes follow
 130 the mass point with the flow in the matrix and dispersed phases. The method to
 131 calculate the flow field at time step $n + 1$ based on that at time step n was as follows. If
 132 we assume that the coordinate value of a certain node is \mathbf{X} and the velocity vector is \mathbf{v} ,
 133 the coordinate value of the node at step $n + 1$ was determined by the central difference
 134 method given by equation (6).

$$135 \quad \mathbf{X}_{n+1} = \mathbf{X}_n + \frac{\mathbf{v}_{n+1} + \mathbf{v}_n}{2} \Delta t \quad (6)$$

136 where subscripts n and $n + 1$ indicate the values at the n and $n + 1$ steps, respectively,
 137 and Δt is the time between consecutive steps.

138 To calculate the velocity field, a mesh that was composed of each node of $n + 1$
 139 steps was used to calculate equation (7) by the Galerkin FEM;

$$140 \quad -\nabla p + 2\eta_r \nabla \cdot \mathbf{D}_{new} = -\nabla \cdot \boldsymbol{\tau} + 2\eta_r \nabla \cdot \mathbf{D}_{old} \quad (7)$$

141 where the reference viscosity η_r was a calculation parameter that can be set arbitrarily.
 142 η_r was determined by the stress and velocity of the field [29]. The subscripts *old* and
 143 *new* represent the known and unknown values, respectively. In the iterative calculation,
 144 $\boldsymbol{\tau}$ and \mathbf{D} on the right of equation (7) substituted the values obtained in the previous
 145 calculation, and the procedure to calculate new values of unknown variables on the left
 146 side was repeated. In this analysis, a decoupled method was used, in which stress and
 147 velocity were solved separately and substituted alternately. Square elements with nine
 148 velocity nodes and four pressure nodes were used. To calculate the viscoelastic stress, a
 149 short time step was set according to the relaxation time, and the constitutive equation
 150 was integrated by the Runge–Kutta method with the stress of n steps as an initial value,
 151 and the stress value at the $n + 1$ step was obtained.

152 At this multiphase flow analysis, we assumed no slippage at the interface.
 153 Therefore, the velocity is continuous at the interface, although other physical quantities,
 154 such as the velocity gradient, stress, and pressure, are discontinuous. For this reason,
 155 double nodes were arranged at the interface, in which different values of the physical
 156 quantities were used [30]. For the velocity analysis, however, the same nodes were
 157 shared for the matrix and dispersed phases to maintain the surface-force continuity. As

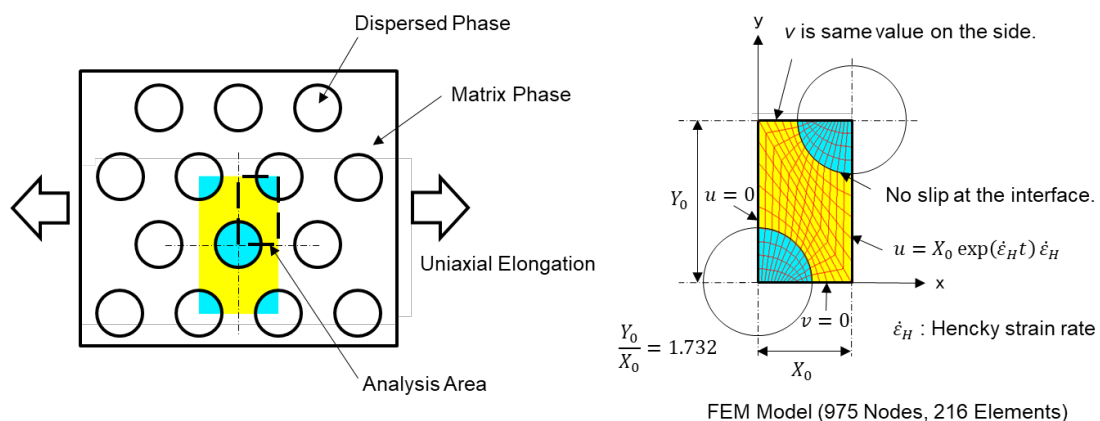
158 described above, the prediction and correction of the velocity, the coordinates of the
 159 nodal point, and the stress were repeated until the calculated value converged, and then
 160 the process shifted to the next step (time).

161

162 3.3 Analytical model

163 By assuming a simplified initial structure shown in Figure 1, the
 164 two-dimensional flow analysis was performed under uniaxial elongational flow of
 165 two-phase materials. A local part was cut because of the periodicity and symmetry. Then
 166 the unit cell in Figure 1 was analyzed. By assuming a fine-grained hexagonal lattice of
 167 the dispersed phase as the initial morphology, a vertical rectangular model was set.

168



170 **Figure 1.** Simplified two-dimensional model of two-phase elongational flow.

171

172 Figure 1 represents the model with 30% of the dispersed phase. In the model
173 with 15% dispersed phase, the radius is reduced further in accordance with the volume
174 fraction. This model allows dimensionless analysis; i.e., the absolute value of the
175 domain size does not affect the analysis result because the surface tension is not
176 considered. Here, a velocity boundary condition with a fixed amount was set in the x
177 direction only at the right side of the analysis region, and the velocities in the direction
178 perpendicular to the boundary plane along the x and y axes were set to zero. Because the
179 x direction velocity at the right side of the analysis area was set, the Hencky strain rate
180 $\dot{\epsilon}_H$ of the field was a constant. As a result, the boundary moved with an exponential
181 function. A two-dimensional flow analysis was performed by assuming that the physical
182 quantities were constants in the depth direction z , and a compression strain rate of $\dot{\epsilon}_H /$
183 2 was set uniformly in the z direction. Therefore, the field deformation became uniaxial
184 elongation. At the boundary of the upper side of the analysis area, the velocity in the y
185 direction was set to be unknown but the values were the same in this plane. Because
186 incompressibility was assumed, the velocity was calculated (the elongational strain rate
187 in the y direction was $-\dot{\epsilon}_H / 2$). For the FEM model, as shown in the figure on the right
188 (Figure 1), a mesh with 975 nodes and 216 elements was constructed. As for the time
189 step in unsteady analysis, the time until the Hencky strain reached six was divided into

190 3000 steps for each elongational strain rate. A calculation of the elongational viscosity
191 was obtained by dividing the average value of the normal stress difference in the y
192 direction by the elongational strain rate. The inhomogeneity in the x direction was
193 considered and the elongational viscosity was calculated by dividing the average value
194 of the normal stress differences across the whole analysis region by the elongational
195 strain rate. As a test analysis of the FEM simulation, the elongational viscosity was
196 calculated by setting the same viscoelastic characteristics for the matrix and dispersed
197 phases, and this viscosity was compared with the elongational viscosity of the single
198 material that was calculated directly from the constitutive equation. We confirmed that
199 both methods gave the same results, which shows that the simulation method is reliable.

200

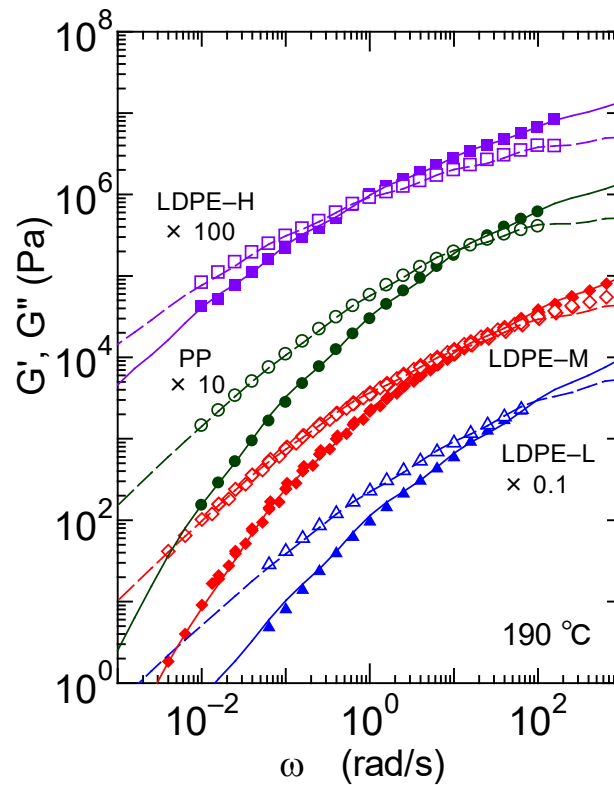
201 **4. Results and Discussion**

202 **4.1 Rheological properties of pure polymers**

203 Figure 2 shows the oscillatory shear moduli, such as the storage modulus G'
204 and loss modulus G'' , as a function of angular frequency ω for the pure samples at 190
205 °C. As shown in the figure, the oscillatory moduli of LDPE-H are higher than those of
206 PP, whereas LDPE-L has lower moduli. The loss moduli of LDPE-M are slightly lower
207 than those of PP. The relaxation spectra that were used for the simulation are estimated

208 from the experimental data, as shown by the solid (G') and dotted (G'') lines.

209



210

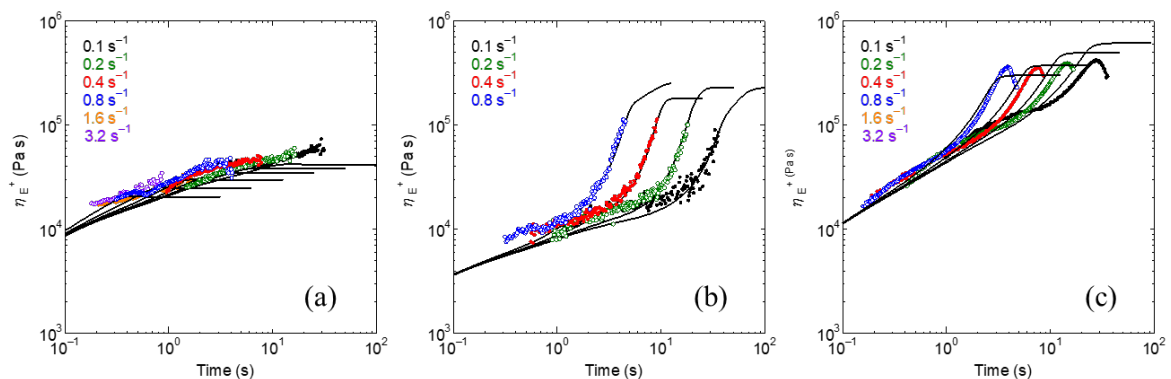
211 **Figure 2.** Experimental (symbols) and calculated (lines) results of the frequency
 212 dependence of shear storage modulus G' (closed symbols and solid lines) and loss
 213 modulus G'' (open symbols and dotted lines) for PP (circles), LDPE-L (triangles),
 214 LDPE-M (diamonds), and LDPE-H (squares) at 190 °C. The vertical axes were shifted.

215

216 Transient elongational viscosities for PP, LDPE-L, and LDPE-H are shown in
 217 Figure 3. The data for LDPE-M were shown elsewhere [10]. The strain hardening
 218 behavior is detected as a steep slope for LDPE-L, and is similar to LDPE-M. In contrast,

219 LDPE-H shows weak strain hardening, i.e., a gentle slope, which is presumed to be
 220 attributed to the difference in the branch structure. Because LDPE-H is produced in a
 221 tubular reactor, the long-chain branch structure is not well-developed compared with the
 222 other LDPE samples that were produced by an autoclave reactor [31-33]. The
 223 elongational viscosities of LDPE-L are lower than those of the pure PP at the beginning
 224 of the elongational flow (short time/strain region) and increase rapidly with time/strain.
 225 Finally, they exceed the values of the pure PP owing to the strain hardening. For
 226 LDPE-H, the elongational viscosities are higher than those of the pure PP from the
 227 beginning of the stretching.

228



229

230 **Figure 3.** Transient elongational viscosity with time at various Hencky strain rates at
 231 190 °C for (a) PP, (b) LDPE-L, and (c) LDPE-H. The experimental data are shown as
 232 circles and the solid lines represent the calculated values.

233

234 The calculated values using the Runge–Kutta method that are derived directly
 235 from the PTT constitutive equation are also shown in Figure 3 by the solid lines. It is
 236 found that the experimental data can be predicted successfully. The non-linear
 237 viscoelastic parameters used in the simulations, such as ξ and ζ , are summarized in
 238 Table 1 with the relaxation spectra calculated from linear viscoelasticity.

239

240 Table 1 Relaxation spectra and PTT model parameters.

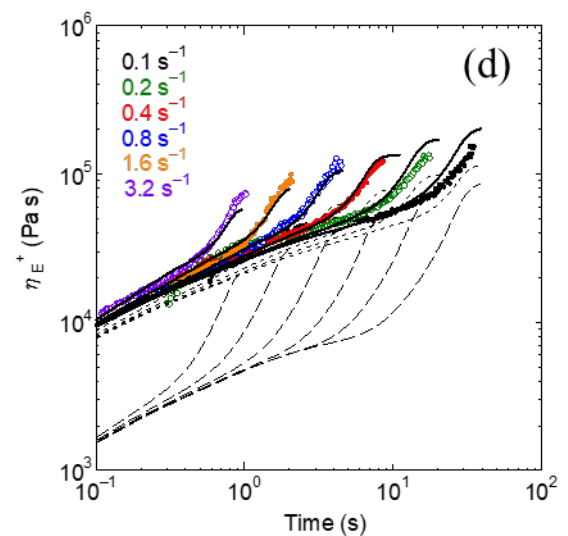
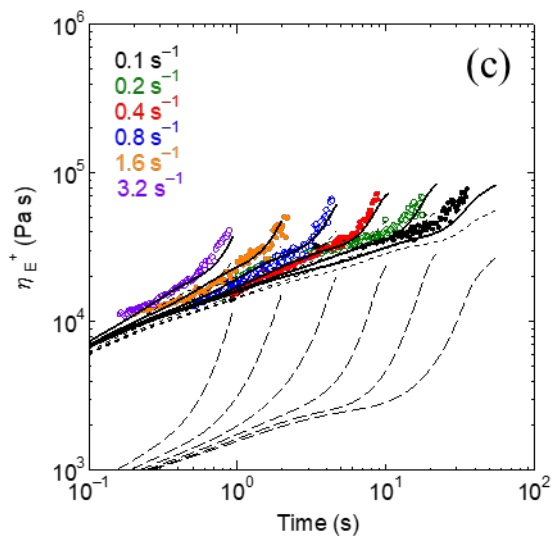
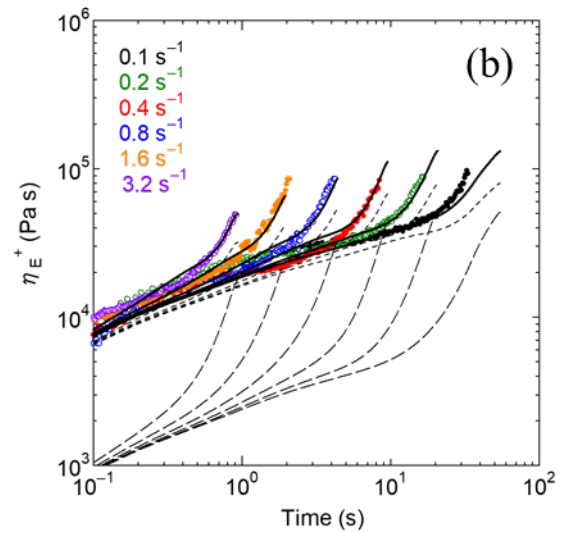
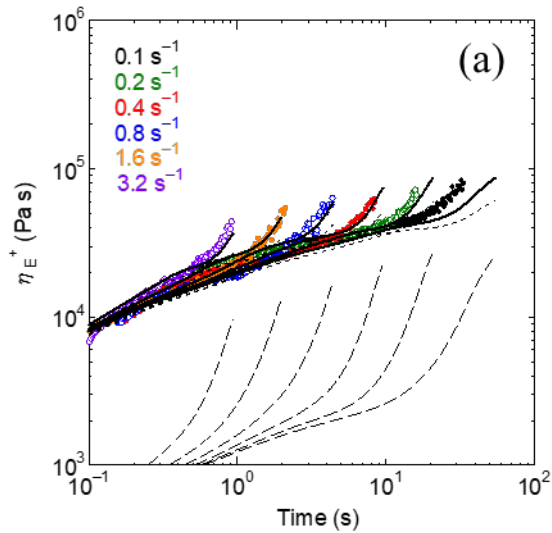
λ (s)	G (Pa)			
	PP	LDPE-L	LDPE-M	LDPE-H
0.001	90000	100000	80000	90000
0.01	62000	38000	40000	53000
0.1	26000	8600	14000	26000
1	4800	1800	3600	11500
10	520	150	400	3200
100	20	10	8	600
1000	-	-	-	80
PTT Model Parameters				
ξ	0.12	0.15	0.15	0.15
ζ	0.5	0.005	0.005	0.08

241

242 **4.2 Uniaxial elongational viscosity of blends**

243 As reported previously [10], PP/LDPE-M (70/30) and (85/15) showed a
 244 marked strain hardening behavior with an intense fashion of PP/LDPE-M (70/30). The
 245 calculated transient elongational viscosities η_E^+ are compared with the experimental
 246 data in Figure 4 with other blends that contain low-viscosity LDPE-L and high-viscosity

247 LDPE-H. The contributions of PP and LDPE to the elongational viscosity, calculated
248 from the stress distribution generated in the two materials, are also indicated in the
249 figure. First, both blend samples, i.e., PP/LDPE-L (70/30) and PP/LDPE-H (70/30),
250 show a clear strain hardening behavior, which is similar to the PP/LDPE-M blends.
251 Second, it was confirmed that the calculation predicts the results.
252



254 **Figure 4.** Transient elongational viscosity η_E^+ with time at various Hencky strain rates
255 at 190 °C for (a) PP/LDPE-M (85/15), (b) PP/LDPE-M (70/30), (c) PP/LDPE-L (70/30),
256 and (d) PP/LDPE-H (70/30). The solid lines represent the numerical results. The
257 contributions of the stress generated in PP (dotted lines) and LDPE (dashed lines) are
258 also indicated.

259

260 When uniaxial elongational flow is applied to a blend having sea-island
261 structure with soft dispersion, the spherical dispersed droplets are elongated to the flow
262 direction and turns into prolonged shape. Then, the interaction between dispersed
263 droplets must be taken into consideration eventually. If this situation is strictly and
264 numerically analyzed using a single domain, the two-dimensional axisymmetric
265 problem occurs, and therefore, a three-dimensional analysis is required. In the present
266 study, however, this phenomenon is approximated by describing in a 2D rectangular
267 coordinate system having sheet-like or ribbon-like dispersed (2D) droplets. Although
268 the error caused by this approximation will be evaluated in near future as compared with
269 the exact 3D model, it is expected that similar results are obtained by both models for
270 the deformation mode and the growth of stress balance around the dispersed droplets. In
271 fact, it was confirmed that the calculation of the approximated model successfully

272 predicts the experimental data of the uniaxial elongational viscosities as shown in
 273 Figure 4, suggesting that this model is practically effective.

274 Here, the transient elongational viscosity of the blend material is estimated by a
 275 simple mixing rule and compared with the calculation result of the FEM analysis.
 276 Assuming the affine deformation of the dispersed phase, the transient viscosity of the
 277 mixture can be estimated by the following simple equation;

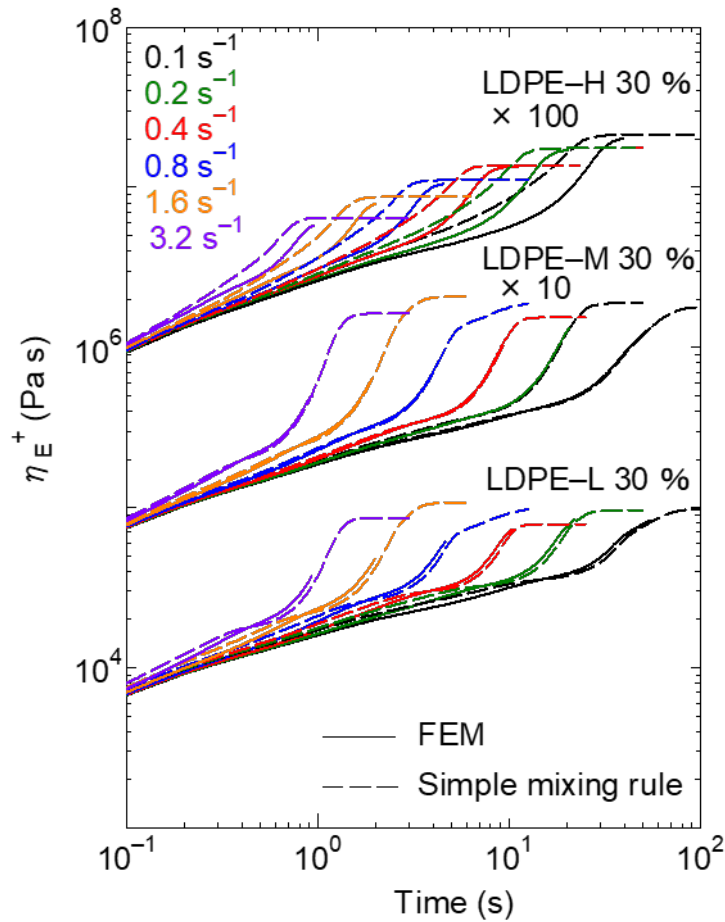
$$278 \quad \eta_E^+(t, \dot{\epsilon}_H) = \phi_c \eta_{cE}^+(t, \dot{\epsilon}_H) + \phi_d \eta_{dE}^+(t, \dot{\epsilon}_H) \quad (8)$$

279 where η_E^+ , η_{cE}^+ , and η_{dE}^+ are the elongational viscosities of the mixture, continuous
 280 phase, and dispersed phase, and ϕ_c and ϕ_d are the volume fractions of the continuous and
 281 dispersed phases, respectively.

282 The elongational viscosity of the mixture was estimated by equation (8) using
 283 the calculated elongational viscosities of the single materials. As shown in Figure 5, it
 284 was found that similar results to the FEM calculation were obtained for PP/LDPE-M,
 285 suggesting that the simple mixing rule is effective when the constituent materials show
 286 similar viscosities. However, differences appear for the other blends. When the
 287 dispersed phase has lower viscosity, i.e., PP/LDPE-L, the strain hardening occurs earlier
 288 for the FEM simulation. For the blend system, the internal strain of the dispersed
 289 droplets develops more quickly than the external strain, as will be mentioned later with

290 the discussion on structure change. In the case that the dispersed phase has higher
291 viscosity, i.e., PP/LDPE-H, in contrast, the deformation of the dispersed droplets does
292 not catch up with the external strain. Consequently, the strain hardening occurs at a
293 longer time (larger strain) than the result by the simple mixing rule. Furthermore, the
294 viscosity levels in the strain hardening region are considerably lower than those by the
295 simple mixing rule. This is attributed to the low aspect ratio of dispersed LDPE-H.
296 Batchelor [11] and Mewis and Metzner [12] clarified that the enhancement of
297 elongational viscosity by fiber addition is pronounced with an increase in fiber aspect
298 ratio.

299



300

301 **Figure 5.** Comparison of elongational viscosities predicted by the finite element method
 302 (solid lines) and by the simple mixing rule (dashed lines).

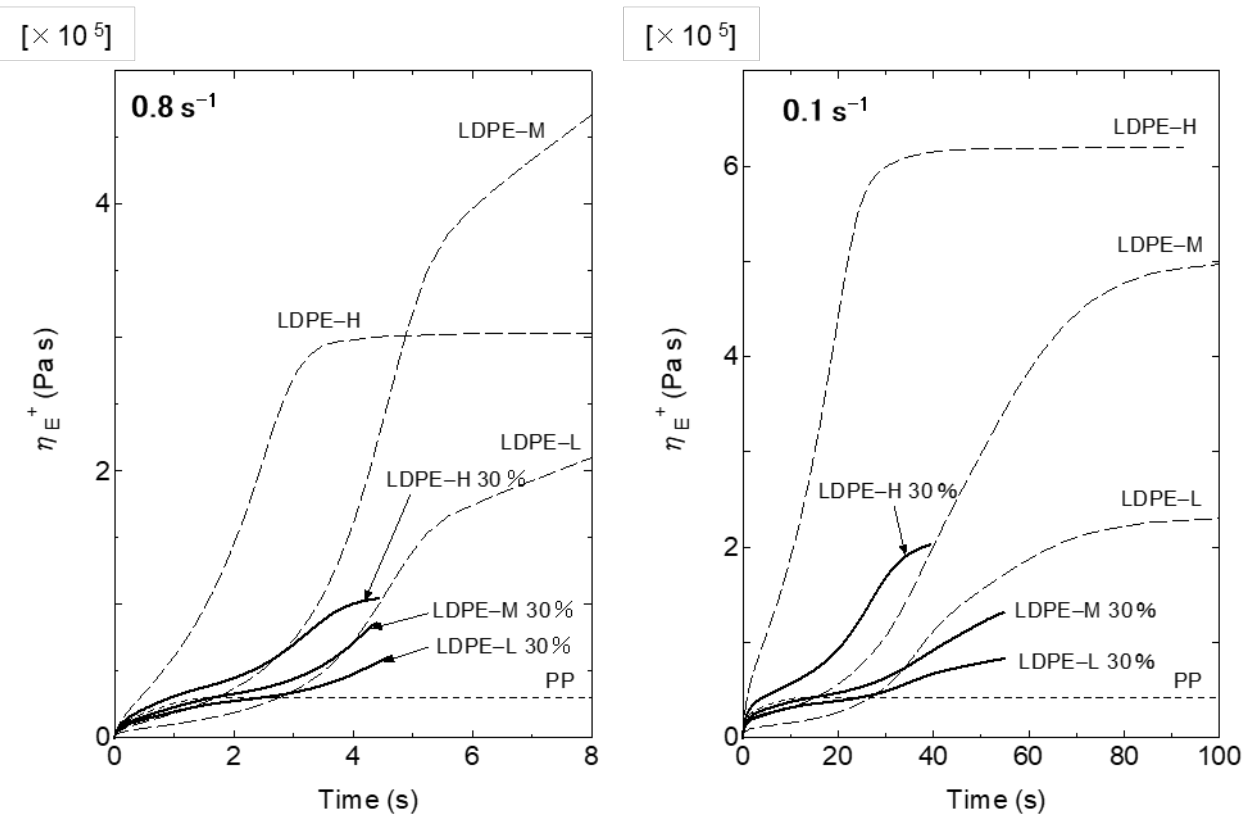
303

304 The contribution of the continuous phase to the elongational viscosity for the
 305 blends increases in the final stage in each system as shown in Figure 4. This indicates
 306 that there is indeed an effect of non-affine deformation of the continuous phase, i.e.
 307 higher elongation strain rate and/or higher normal stress difference in some area. Figure
 308 4 also indicates that the contribution of the dispersed phase increases rapidly in the large

309 deformation area, suggesting that the dispersed phase eventually shows pseudo affine
310 deformation.

311 To clarify the difference in the strain hardening for the blend samples
312 quantitatively, the calculated values of the blends with 30% LDPE are shown in Figure
313 6 with those of the pure components, i.e., PP and LDPE. As compared with the
314 PP/LDPE-H, both PP/LDPE-M and PP/LDPE-L show strain hardening in the long time
315 (large strain) region; i.e., the strain hardening is delayed. This is reasonable because a
316 large strain is required for LDPE-L and LDPE-M to show a higher elongational
317 viscosity than PP, although the difference in onset of strain hardening between
318 PP/LDPE-M and PP/LDPE-L is minimal, and will be discussed later. In contrast, strain
319 hardening occurs in the short time region for the blend with LDPE-H. This is owing to
320 the prompt stress growth of LDPE-H. Even though strain hardening of the dispersed
321 droplets in PP/LDPE-H is delayed from that of LDPE-H alone, the strain hardening still
322 occurs in the shorter time region as compared with the other blends.

323



324

325 **Figure 6.** Calculated elongational viscosity of PP, LDPE, and the blend with 30% LDPE.

326 (Left) $\dot{\epsilon}_H = 0.8 \text{ s}^{-1}$ and (right) $\dot{\epsilon}_H = 0.1 \text{ s}^{-1}$.

327

328 4.3 Development of morphology and stress distribution

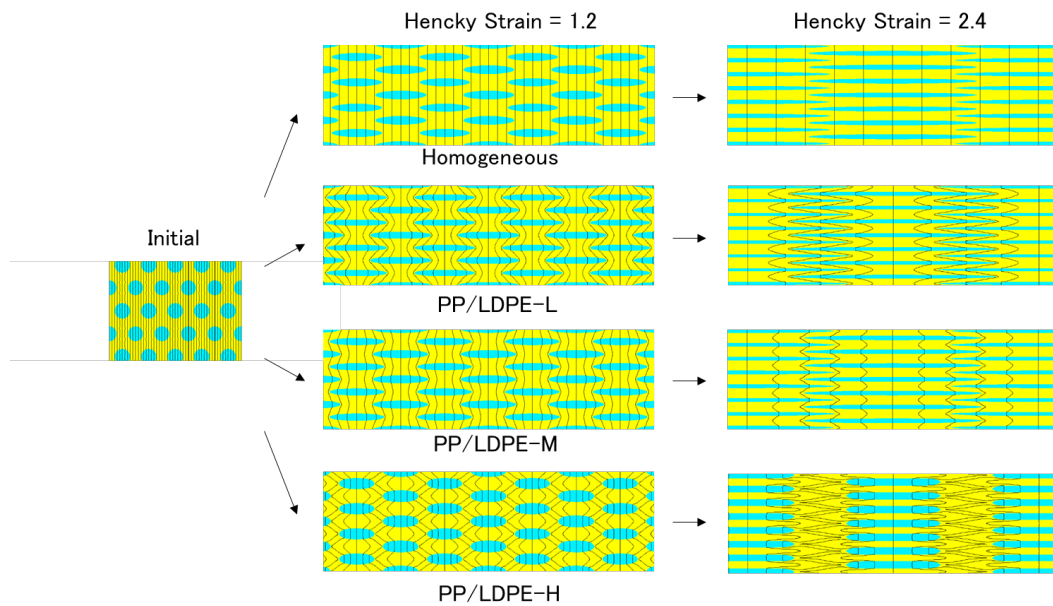
329 As commented previously, the shape of the dispersed phase has a strong impact

330 on the rheological behavior under elongational flow. Therefore, the structure

331 development of the blends containing 30% of LDPE is calculated. Figure 7 shows the

332 structures during stretching at Hencky strains ϵ_H of 1.2 and 2.4.

333



334

335 **Figure 7.** Numerical results of structure development under uniaxial elongational flow

336 for blends with 30% LDPE.

337

338 In the figure, longitudinal lines at the initial state are inserted periodically to

339 comprehend the deformation easily. Furthermore, the structures are magnified to see the

340 lines clearly at Hencky strains of 1.2 and 2.4. For the homogeneous material, in which

341 continuous and dispersed phases are the same substance, both phases deform in the

342 same way. Therefore, the lines remain straight with an increase in the distance as the

343 deformation progresses. When the dispersed phase shows a different viscoelasticity

344 from the continuous phase, the lines become distorted. For PP/LDPE-L, the dispersions

345 deform more rapidly than the external deformation in the early stage of elongation,

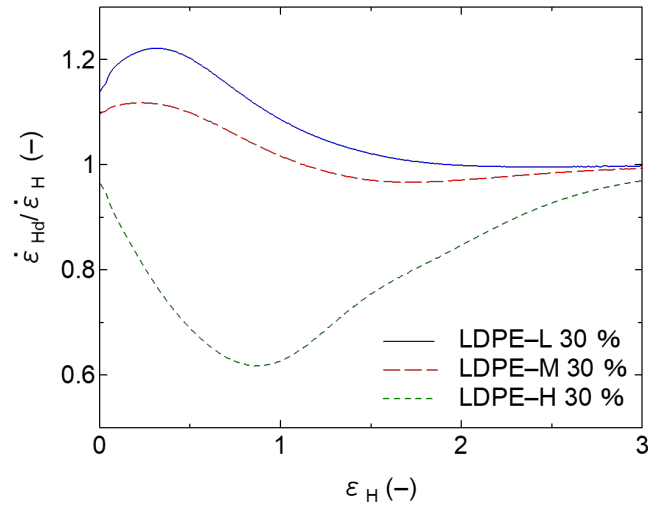
346 which leads to prolonged droplets promptly. Such a structure development of blends

347 with a sea-island morphology has been reported previously by advanced research
348 groups [15,19,34]. Similarly, the LDPE-M dispersions, which show a slightly lower
349 viscosity than the continuous PP in the short time region, deform more than the external
350 strain, although their deformation is smaller than that of the LDPE-L. Because LDPE-L
351 shows a larger deformation in the blend, the onset strain to show strain hardening is not
352 so different from that for PP/LDPE-M (Figure 6). In contrast, the LDPE-H deformation
353 is delayed because of their higher viscosity than the continuous PP. Because the
354 deformation of the dispersed phase cannot catch up with the continuous one for
355 PP/LDPE-H, the LDPE-H droplets do not overlap each other even under a large
356 deformation, and thus nonuniformity appears in the width direction. In this analysis
357 model, periodic configuration is assumed, and the dispersed droplets are arranged
358 straight vertically. Since the dispersed phase is not so hard for PP/LDPE-H, the
359 elongational viscosity could be predicted by averaging the stress in the width direction.
360 However, if the viscosity of a dispersed phase is too high to be undeformable during
361 elongational flow; i.e., dispersed particles behave as rigid body like inorganic fillers,
362 this analytical model will not be applicable.

363 Figure 8 shows the ratio of Hencky strain rate of a dispersion $\dot{\epsilon}_{Hd}$ to the
364 external strain rate $\dot{\epsilon}_H$, i.e., $\dot{\epsilon}_{Hd} / \dot{\epsilon}_H$, as a function of the external strain for the blends

365 with 30% LDPE. The strain rate of a dispersion is determined by $(dR_1/dt) / R_1$, where R_1
 366 is the major radius of the dispersion.

367



368

369 **Figure 8.** Ratio of the Hencky strain rate of the dispersion to the external strain rate,
 370 $\dot{\epsilon}_{Hd} / \dot{\epsilon}_H$, as a function of the external strain ϵ_H for PP/LDPE (70/30) at $\dot{\epsilon}_H = 0.8 \text{ s}^{-1}$.

371

372 Figure 8 shows that the effect of the LDPE species appears in the early stage of
 373 the elongational flow. Furthermore, the direction of the deviation, i.e., upper (larger than
 374 unity) or lower (smaller than unity), is determined by the viscosity ratio of PP to LDPE.
 375 It is interesting to note that the ratio of the blend with LDPE-M is larger than unity
 376 initially, and smaller than unity beyond a strain of 1.1; i.e., the dispersions act as long
 377 rigid fibers.

378

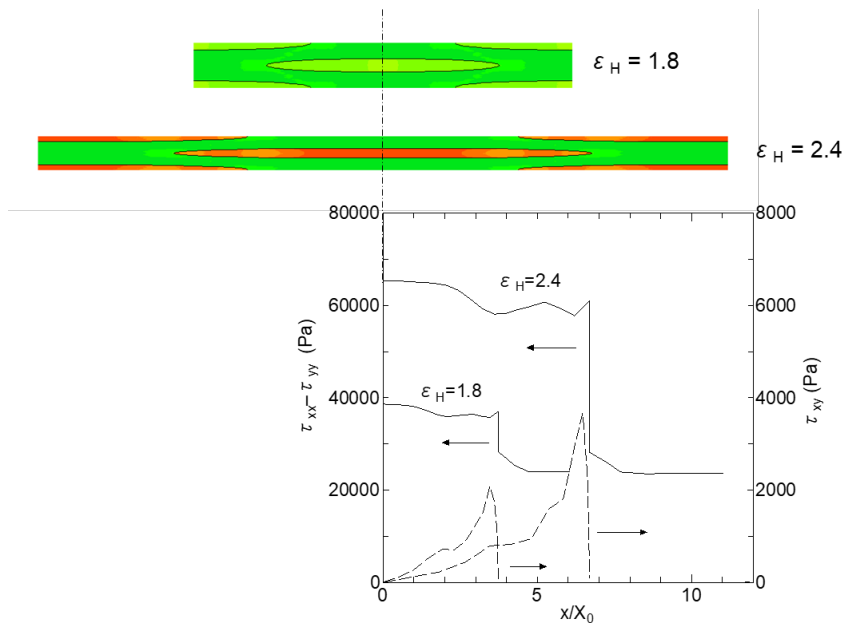
It is also found that the ratios of the strain rates, i.e., $\dot{\epsilon}_{Hd} / \dot{\epsilon}_H$, gradually

379 approaches one for all blends, although the values at the initial stage are determined by
380 the viscosity ratio of PP to LDPE. This result indicates that all systems are approaching
381 affine deformation under the large deformation, which is prominent especially for the
382 blend systems with LDPE-L and LDPE-M. Therefore, the values predicted by the
383 simple mixing rule were closed to those of the FEM analysis as shown in Figure 5.

384 Figure 9 shows the distributions of shear stress τ_{xy} at the boundary surface of a
385 dispersion and tensile stress $\tau_{xx} - \tau_{yy}$ at the center of a dispersion in the x direction during
386 stretching at $\dot{\varepsilon}_H = 0.8 \text{ s}^{-1}$ for PP/LDPE-M (70/30). The shear stress shows the
387 maximum at the end of the elliptical dispersion, and decreases toward the center, which
388 balances the tensile stress that is generated in the dispersion. With an increase in the
389 aspect ratio of the dispersion, the shear stress, especially near the end parts of the
390 dispersion, is enhanced significantly. Moreover, the elongational stress in the dispersion
391 is high as revealed by the previous researches [35,36]. As a result, the apparent
392 elongational viscosity for the whole system is enhanced. Such a stress distribution was
393 also confirmed in the elastic deformation analysis for a composite material with long
394 cylindrical fibers [37,38]. In the present system, however, a large elongational stress is
395 detected for the whole of the LDPE dispersion, which is different from the stress
396 distribution in the cylindrical fiber composite. This phenomenon occurs because the

397 cross-sectional area of the dispersion decreases toward the end, which leads to a high
 398 elongational stress near the end [39].

399



400

401 **Figure 9** Distributions of tensile stress at the center of the dispersed phase and shear
 402 stress at the surface of the dispersed phase at $\epsilon_H = 1.8$ and 2.4 during elongation flow at
 403 $\dot{\epsilon}_H = 0.8 \text{ s}^{-1}$ for PP/LDPE-M (70/30).

404

405 It is found that the elongation stress acting on the dispersed phase is
 406 considerably higher than the shear stress at the surface of the dispersion. When the
 407 aspect ratio increases, the interfacial area of the dispersed droplets increases greatly
 408 with the decrease in the vertical cross-sectional area. As a result, dispersed droplets with
 409 high viscosity can be deformed affinely. Figure 9 also shows that the shear stress is low

410 near the center of the dispersed droplet. A similar situation was detected also for a
411 composite system with long fibers, suggesting that the center area is affinely deformed.
412 Although the strain hardening occurs in the dispersion under a large strain, the
413 dispersion shows pseudo affine deformation following the external strain rate. Thus,
414 high elongational stress is developed in the dispersed phase, which directly contributes
415 to the increase in the elongational viscosity of the blend. This situation is magnified
416 with increase in the volume fraction of the dispersed phase.

417

418 The simulation result indicates that the elongational viscosity of the PP/LDPE
419 blend systems can be controlled by the ratio of the elongational viscosities between PP
420 and LDPE and the strain hardening behavior of LDPE. When the LDPE shows a lower
421 viscosity, it turns into a fibrous shape promptly. Then, a steep increase in elongational
422 viscosity, i.e., pronounced strain hardening, is provided for the blend after stretching to
423 some degree; i.e., the strain hardening is delayed. When the strain hardening is required
424 in the early stage of flow, e.g., reduction of neck-in level at T-die extrusion, LDPE that
425 has a slightly higher shear viscosity with a marked strain hardening in the elongational
426 viscosity is recommended. In the case of foaming, LDPE with a low shear viscosity
427 would be recommended to show a large expansion ratio because the strain hardening

428 occurs at a large strain.

429

430 **5. Conclusions**

431 The effect of LDPE addition on the rheological properties of PP under uniaxial
432 elongational flow is investigated. The LDPE addition is found to provide strain
433 hardening in the transient elongational viscosity for PP although LDPE is the dispersed
434 phase. Moreover, the experimental results were predicted by the numerical simulation
435 by using the PTT model with multiple relaxation modes by assuming the symmetric
436 geometry with a periodic structure. The transient elongational viscosity for pure LDPE
437 determines the critical strain to show strain hardening and the magnitude of strain
438 hardening for the blends. When the shear viscosity of LDPE is lower than that of PP, the
439 strain hardening appears later with a steep slope, where LDPE dispersions have a high
440 aspect ratio. In contrast, the blend with LDPE with a higher viscosity shows strain
441 hardening in the early stage of the flow. These results obtained in this study will be
442 useful to select an appropriate LDPE as a processing modifier for PP in real processing
443 operations.

444

445 **References**

- 446 1. Yamaguchi, M.; Miyata, H. *Polym. J.* **2000**, *32*, 164-170.
- 447 2. Sugimoto, M.; Masubuchi, T.; Takimoto, J.; Koyama, K. *Macromolecules* **2001**, *34*,
448 6056-6063.
- 449 3. Kurose, T.; Takahashi, T.; Sugimoto, M.; Taniguchi, T.; Koyama, K. *Nihon Reoroji*
450 *Gakkaishi*, **2005**, *33*, 173-182.
- 451 4. Yamaguchi, M.; Wakabayashi, T. *Adv. Polym. Technol.* **2006**, *25*, 236-241.
- 452 5. Mieda, N.; Yamaguchi, M. *J. Non-Newtonian Fluid Mech.* **2011**, *166*, 231-240.
- 453 6. Yokohara, T.; Nobukawa, S.; Yamaguchi, M. *J. Rheology* **2011**, *55*, 1205-1218.
- 454 7. Yamaguchi, M.; Yokohara, T.; Ali, M. A. B. *Nihon Reoroji Gakkaishi*, **2013**, *41*,
455 129-135.
- 456 8. Siriprumpoonthum, M.; Nobukawa, S.; Satoh, Y.; Sasaki, H.; Yamaguchi, M. *J.*
457 *Rheology* **2014**, *58*, 449-466.
- 458 9. Seemork, J.; Sako, T.; Ali, M. A. B.; Yamaguchi, M. *J. Rheology* **2017**, *61*, 1-11.
- 459 10. Fujii, Y.; Nishikawa, R.; Phulkerd, P.; Yamaguchi, M. *J. Rheology* **2019**, *63*, 11-18.
- 460 11. Batchelor, G. K. *J. Fluid Mech.* **1971**, *46*, 813-829 (1971).
- 461 12. Mewis, J.; Metzner, A. B. *J. Fluid Mech.* **1974**, *62*, 593-600.
- 462 13. Laun, H. M. *Colloid Polym. Sci.* **1984**, *262*, 257-269.
- 463 14. Toose, E. M.; van Damme, R. M. J.; van den Ende, H. T. M.; Geurts, B. J.; Kuerten,
464 J. M. G. *J. Non-Newtonian Fluid Mech.* **1995**, *60*, 129-154.

- 465 15. Delaby, I. Ernst, B.; Froelich, D.; Muller, R. *Polym. Eng. Sci.* **1996**, *36*, 1627-1635.
- 466 16. Ramaswamy, S.; Leal, L. G. *J. Non-Newtonian Fluid Mech.* **1999**, *85*, 127–163.
- 467 17. Ramaswamy, S.; Leal, L.G. *J. Non-Newtonian Fluid Mech.* **1999**, *88*, 149–172.
- 468 18. Hooper, R. W.; de Almeida, V. F.; Macosko, C. W.; Derby, J. J. *J. Non-Newtonian*
469 *Fluid Mech.* **2001**, *98*, 141–168.
- 470 19. Cristini, V.; Hooper, R. W.; Macosko, C. W.; Simeone, M.; Guido, S. *Ind. Eng.*
471 *Chem. Res.* **2002**, *41*, 6305-6311
- 472 20. Mukherjee, S.; Sarkar, K. *J. Non-Newtonian Fluid Mech.* **2009**, *160*, 104–112.
- 473 21. Cardinaels, R.; Afkhami, S.; Renardy, Y.; Moldenaers, P. *J. Non-Newtonian Fluid*
474 *Mech.* **2011**, *166*, 52–62.
- 475 22. Skartilien, R.; Sollum, E.; Akselsen, A. Meakin, P. *Rheol. Acta* **2002**, *51*, 649-673.
- 476 23. Isbassarov, D.; Rosti, M. E.; Ardekani, M. N.; Sarabian, M.; Hormozi, L. B.;
477 Tammissola, O. *Int. J. Numerical Methods Fluids* **2018**, *88*, 521-543.
- 478 24. Hwang, W. R.; Hulsen, M. *J. Non-Newtonian Fluid Mech.* **2006**, *136*, 167-178.
- 479 25. D'Avino, G.; Maffettone, P. L.; Hulsen, M. A.; Peters, G. W. M. *J. Comp. Phys.*
480 **2007**, *226*, 688-711.
- 481 26. Ahamdi, M.; Harlen, O. G. *J. Comp. Phys.* **2008**, *227*, 7543-7560.
- 482 27. Phan-Thien, N.; Tanner, R. I. *J. Non-Newtonian Fluid Mech.* **1977**, *2*, 353-365.

- 483 28. Otsuki, Y.; Umeda, T.; Tsunori, R.; Shinohara, M. *Nihon Reoroji Gakkaishi* **2005**, *33*,
484 9-16.
- 485 29. Otsuki, Y.; Kajiwara, T.; Funatsu, K. *Polym. Eng. Sci.* **1999**, *39*, 1969-1981.
- 486 30. Matsunaga, K.; Kajiwara, T.; Funatsu, K. *Polym. Eng. Sci.* **1998**, *38*, 1099-1111.
- 487 31. Tackx, P.; Tacx, J. C. J. F. *Polymer* **1998**, *39*, 3109-3113.
- 488 32. Yamaguchi, M.; Takahashi, M. *Polymer* **2002**, *42*, 8663-8670.
- 489 33. Mieda, N.; Yamaguchi, M. *Adv. Polym. Technol.* **2007**, *26*, 173-181.
- 490 34. Levitt, L.; Macosko, C. W.; Pearson, S. D. *Polym. Eng. Sci.* **1996**, *36*, 1647-1655.
- 491 35. Goddard, J. D. *J. Non-Newtonian Fluid Mech.* **1976**, *2*, 1-17.
- 492 36. Pipes, R. B.; Hearle, J. W. S.; Beaussart, A. J.; Sastry, A. M.; Okine R. K. *Compos.*
493 *Mater.* **1991**, *25*, 1204-1217.
- 494 37. Carrara, A. S.; McGarry, F. J. *J. Comp. Mat.* **1968**, *2*, 222-243.
- 495 38. Harris, B., *Engineering Composite Materials*, 2nd ed. **1999**, Maney Publishing,
496 Leeds.
- 497 39. Goh, K. L.; Mathias, K. J.; Aspden, R. M.; Hukins, D. W. H. *J. Mater. Sci.* **2000**, *35*,
498 2493-2497.
- 499